LOCAL DAMPING IDENTIFICATION FROM SPACECRAFT SINE TEST

G. Ladurée[1], A. Carpine[1], R. Redondo[2]

[1] Thalès Alenia Space
100 Boulevard du Midi, 06156 Cannes la Bocca
France

[2] Centre National d'Etudes Spatiales
18, avenue Edouard Belin
31401 Toulouse Cedex 4
France

OVERVIEW

A thorough knowledge of the damping in a structure as well as a relevant method to model it constitutes necessary steps for reliable dynamic analyses. A bad knowledge of the damping may lead to over-estimate or under-estimate the dynamic responses inside the spacecraft with all the potential serious consequences on the program and/or the service life of the satellite.

This paper describes an ongoing development with CNES of a methodology based on relevant database exploitation for deriving structural damping of substructures. The final purpose, still to be completed, is to define simple empirical rules for predicting structural damping per type of substructures.

1. INTRODUCTION

 The proposed methodology relies on the exploitation of spacecraft sine tests and the use of correlated FEM to identify local structural damping of substructures or per type of substructures. The identification process is based on the relationship between the structural modal damping identified from the sine test and the associated modal strain energy per substructures calculated with the FEM. Then the structural damping of substructures participating to the excited modes are obtained by solving a discrete inverse problem which is, by nature, an ill-posed problem (under or over-constraint and ill-conditioned matrix).

A regularization procedure based on Tikhonov method is proposed and detailed in order to identify realistic values of damping. This procedure has been implemented and automated in order to extract systematically and rapidly local damping and be able to highlight influent parameters.

This whole identification process has been applied on several types of spacecraft : candidates have been chosen among the SPACEBUS family for telecommunication satellites and among PROTEUS family for observation satellites. The first step consists in the identification of experimental modal parameters from the sine test (resonant frequencies, modal damping and associated mode shapes). Then the next step is the correlation of the corresponding FEM in terms of frequency and MAC followed by the computation of the modal strain energy per substructures. Finally the inverse problem was solved using the regularization procedure.

2. METHODOLOGY

The selected approach is based on the expression of modal structural damping η_k with respect to subsystems structural damping η_s and the percentage of modal strain energy associated to these subsystems $(\tau_k)_s$

$$(1) \qquad \eta_k = \sum_s \eta_s (\tau_k)_s$$

The methodology is composed of the following steps :

- Modal identification from measured FRFs (Frequency Response Functions) during system sine tests. It may be reduced to natural frequencies, modal damping values and modal effective parameters. The RTMVI has been used.

- FEM updating. The usual criteria of frequency error and MAC have been used as objective functions.

- Modal strain energy calculation for the subsystems participating to the identified modes.

- Extraction of structural damping of the subsystems considered, by solving the inverse problem given by the equation (1).

Equation (1) constitutes the typical example of inverse problem where one wants to estimate a physical property *x* that is not accessible through experiment thanks to the measure of another physical property *b* and by the knowledge of a mathematical model of the direct problem giving explicitly *b* knowing *x* (noted symbolically A(x)=b).

2.1. Modal identification

The first step consists in a classical modal identification process, which is already an inverse problem. Before processing to the identification itself, a certain number of questions have to be answered properly to be confident in the results.

2.1.1. Test level choice

The type of test to be chosen for the identification depends on the final searched information. The choice can be made between low level, intermediate level or qualification runs. The advantage of low level runs reside a priori in the absence of nonlinearities that can facilitate the identification process. But these runs can also be prone to excessive noise. On the contrary, the qualification runs lead often to consider higher damping due to non-linear behaviour of the specimen or boundary conditions (physical damping mechanisms are intrinsically complex and nonlinear). In the present study, the desired information is the damping of substructures with a final aim of prediction. It has been consequently judged that the qualification runs were the best candidates as they can provide the most interesting result for the system engineer.

2.1.2. Adequacy of test data

The signal quality of experimental data is fundamental for the proper measurement of the modal parameters to be used for the mathematical model validation.

Low frequency check primarily provides confirmation of the proper sensor sensitivity setting which is an indication of the correct measurement of the response amplitude. From the measured FRF the low frequency response amplitude (at least for the measurement in the same excitation directions) can be automatically compared with the nominal rigid-body input and corrective actions applied if necessary. In practice, the low frequency check involves comparing the error between the measured FRF and the second-order function $a + b\omega^2$ where a provides the rigid body component and b the dynamic amplification contribution [4].

Sensor orientation check ensures that the modal parameters extraction will not be based on erroneous information. This check controls automatically the orientation and sign of the accelerometers. It is done by comparing in all 3 directions the low-frequency responses of the accelerometers with the rigid body motion derived from the model's geometry [4].

2.1.3. Modal identification

The modal identification process has been performed with the RTMVI method [5] that reduces the identification from measured FRFs to natural frequencies f_k, damping η_k and modal effective parameters MEP_k. Usual modal shapes may be recovered through the modal effective parameters.

In practice, these parameters are extracted from the imaginary part of the FRFs. As explained in [5], the imaginary part :

- contains amplitude and sign information
- is closer to the peaks of the natural frequencies
- minimizes the influence of close modes
- is not influenced by static and inertia terms as the real part is.

It has to be noticed that the damping is the most difficult parameter to extract. It is directly related to the sharpness of the peak and its identification is very sensitive.

2.2. Test-Analysis comparison

The comparison between the test measures and the FEM modal analysis consists in :

- Comparison of natural frequencies, modes shapes and modal effective parameters
- Mode pairing using MAC The main spacecraft and subsystems modes are identified.

2.3. FEM updating

Once compared with the test results, the FEM has to be updated in order to minimize some observed discrepancies in natural frequencies or mode shapes for the identified modes.

This updating process was performed through the modification of unitless design coefficient on the stiffness matrix (the mass matrix has been considered as sufficiently representative) and has been done through a robust and efficient optimization strategy using the Simplex algorithm [6].

The value of the resulting design coefficient was bounded in order to limit the stiffness variation to physical and realistic modification.

2.4. Modal strain energy calculation

If the updating process is judged successful, the FEM is considered as sufficiently representative in mass and stiffness to be used for the modal strain energy calculation. The calculation of $(\tau_k)_s$ involves each identified modes k and the associated substructures or subsystems s.

A threshold criterion has been defined to limit the number of zones and to avoid introducing some small values behaving potentially as numerical perturbation in the inverse problem resolution. The threshold was fixed to 1% of modal strain energy, i.e. the retained zones for the identified modes have more than 1% of strain energy.

It is clear that the number of identified modes and associated zones are generally distinct. The inverse problem to solve is consequently over or under-constrained. In other words, the matrix $[\tau_{ks}]$ of equation (1) is rectangular with $k > s$ or $k \leq s$.

2.5. Extraction of structural damping

The next step is the resolution of the inverse problem to obtain η_s.

2.5.1. Discrete ill-posed problems

Discrete inverse problems like equation (1) can be classified into two categories [3]:

- Problems that have a unique continuous solution x with regard to b. They are said well-posed (in Hadamard sense)

- Problems for which the existence, uniqueness and/or continuity of a solution with regard to the measures are not all verified. Physically, it means that a measure b with its associated uncertainty, can result in a wide range of values of x or that an arbitrarily small perturbation of the data can cause an arbitrarily large perturbation of the solution. The problem is thus said to be ill-posed (in Hadamard sense).

The equation (1) is typically an ill-posed problem because of the uncertainties in $\left[\tau_{ks}\right]$ and η_k, which can be assimilate to small perturbations. These uncertainties have various origins :

- Experimental data contains intrinsically some stochastic behaviour.

- The mathematical model stands for an ideal representation of physics and is funded on simplified assumptions (cabling, equipment, thermal control, boundary conditions…). The updating process is also the result of a mathematical compromise to minimize a defined distance between test and analysis models. The model itself can also be considered as a source of uncertainty.

An important aspect of discrete ill-posed problems is that standard method in numerical linear algebra cannot be used in a straightforward manner to compute such a solution. Instead, more sophisticated methods must be applied in order to ensure the computation of a meaningful solution. One type of methods consists in regularizing the problem, that is to say replacing the initial ill-posed problem by a new one, close to the first one, but well-posed.

2.5.2. Regularization of ill-posed problem

Mathematically, an discrete inverse problem or linear least-squares problem described by the equation :

$$(2) \qquad \min_x \left\|Ax - b\right\|_2 \text{ with } A \in \mathfrak{R}^{mxn}$$

is said to be ill-posed if both of the following criteria are satisfied [2]:

1. The singular value of A decay gradually to zero

2. The ratio between the largest and the smallest nonzero singular values is large

The first criterion indicates that there is no nearby problem with a well-conditioned matrix and with well-determined numerical rank. The second criterion implies that the matrix A is ill-conditioned, i.e. that the solutions are potentially very sensitive to perturbations.

Ill-posed problems are mainly undetermined due to the cluster of small singular values of A. Hence, it is necessary to add further physical information about the solution to stabilize the problem and obtain one unique solution. This is the goal of regularization techniques.

This physical information or constraints will be added to the initial linear least squares problem by requesting to minimize the 2-norm or a semi-norm of the solution. Hence, the side constraint involves the minimization of the following quantity :

$$(3) \qquad \Omega(x) = \left\|Lx\right\|_2$$

where L is a linear operator that can either be the identity matrix or a [p x n] matrix containing p linear physical relationships between the components of the solution x. One important point to notice is that when the side constraint $\Omega(x)$ is introduced, the solution is now a compromise or balance between minimizing $\Omega(x)$ and minimizing the residual norm of equation (2).

The most common form of regularization method is the Tikhonov regularization that expresses the desired solution x_λ as

$$(4) \qquad x_\lambda = \arg \min \left\{ \left\|Ax - b\right\|_2^2 + \lambda^2 \left\|Lx\right\|_2^2 \right\}$$

where the regularization parameter λ controls the relative weight between the minimization of the side constraint and the minimization of the residual norm. A large λ, equivalent to a large regularization, will favour a small solution norm at the cost of a large residual norm and vice versa.

The choice of λ is generally done using the so-called the L-curve method which is a graphical tool plotting the norm of the regularized solution $\left\|Lx\right\|_2^2$ versus the corresponding residual norm $\left\|Ax - b\right\|_2^2$. The solution computed by Thikhonov regularization is optimal in the sense that for a given residual norm, there is no solution with a smaller seminorm than the Thikhonov solution. By locating the corner of the L-curve one can compute an approximation to the optimal regularization parameter λ and thus, compute a regularized solution with a good trade-off between the two types of errors. A large λ will lead to a small solution seminorm at the cost of a large residual norm, while a small λ will have an inverse effect. In other words, λ controls the sensitivity of the regularized solution to perturbations in A and b.
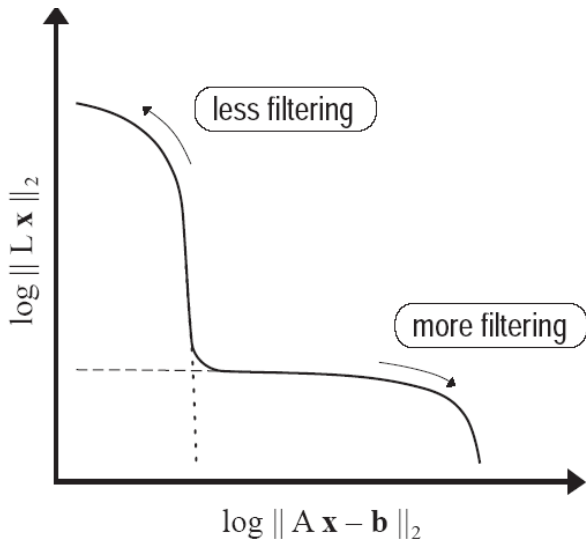
FIG 1.   L-curve principle

Other solutions exist and are generally based on the SVD. The smallest singular values are filtered to avoid propagating or amplifying errors and uncertainties. This filtering can consists in truncating (truncated SVD) the singular values or damping (damped SVD) their effect.

2.5.3. Automation of the regularization method

An automated extraction process has been implemented with the following inputs :

- Manual choice of considered modes or automatic choice with regard to minimal MAC

- Manual choice of zones or automatic choice based on minimal modal strain energy rate.

This procedure has been implemented under Matlab environment.

3. STUDY CASE : SPACEBUS 4000

Several examples have been chosen among the SPACEBUS family for telecommunication satellites and among PROTEUS family for observation satellites. For all cases similar conclusions can be derived. The presented case corresponds to a SPACEBUS 4000. The name of satA will be used for convenience.

3.1. Experimental model

As explained in paragraph 2.1.1, the sine qualification run have been selected to process to the modal identification. The adequacy of test data has been carefully examined (see paragraph 2.1.2) to facilitate and secure the identification process. The resulting number of channels retained after the low frequency checks is presented in TAB 1.

Number of Channels after low frequency checks			
	Direction X	Direction Y	Direction Z
Satellite A	125	170	128

TAB 1.   Valid instrumentation

3.2. Modal identification

The modal identification process described in paragraph 2.1.3 is illustrated hereunder on FIG 2 and TAB 2 for the lateral axis X. The modes below 80 Hz have been extracted from the imaginary parts of the FRFs. Global modes of the spacecraft as local modes of subsystems like the solar arrays or the antennas can thus be identified. Natural frequencies, damping, modal effective parameters and interface parasitic motion indicator have been extracted. This latter parameter is an efficient indicator of the quality of the extracted modes because this motion may degrade significantly the structure's responses and modes.
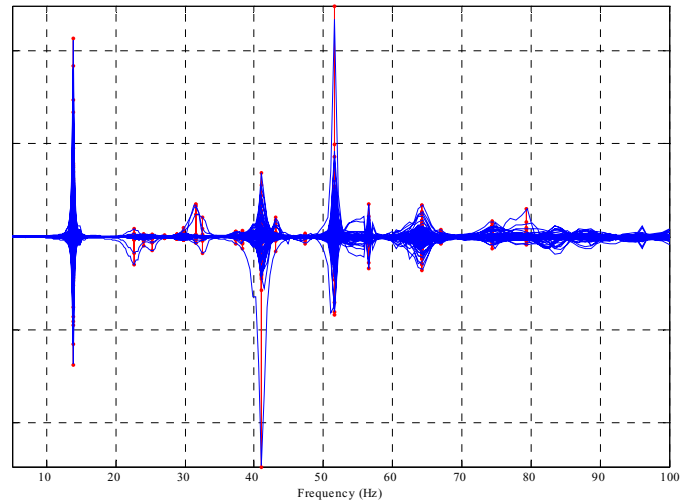
FIG 2.   Modal identification on imaginary parts of FRFs

```
------------------------------
Model: satA_run_x_LF5_OR025
------------------------------
  Mode     Freq.     Damp.    I/F
  (k)      (Hz)      (2z)     (%)
------------------------------
   1       13.89     0.0207    1
   2       22.61     0.0870    0
   3       24.02     0.0766    0
   4       25.26     0.0830    0
   5       27.01     0.0765    0
   6       28.85     0.0503    0
   7       29.79     0.0795    0
   8       31.51     0.0515    0
   9       32.55     0.0437    0
   .
   .
   .
------------------------------
```

TAB 2.   Identified modes, damping and parasitic motion on X axis run

3.3. FEM

The FEM is shown in FIG 3 and described in TAB 3. It is constituted of physical elements and reduced matrix models for large subsystems (solar arrays, reflectors). 172 modes are computed between 12.4 and 80 Hz.
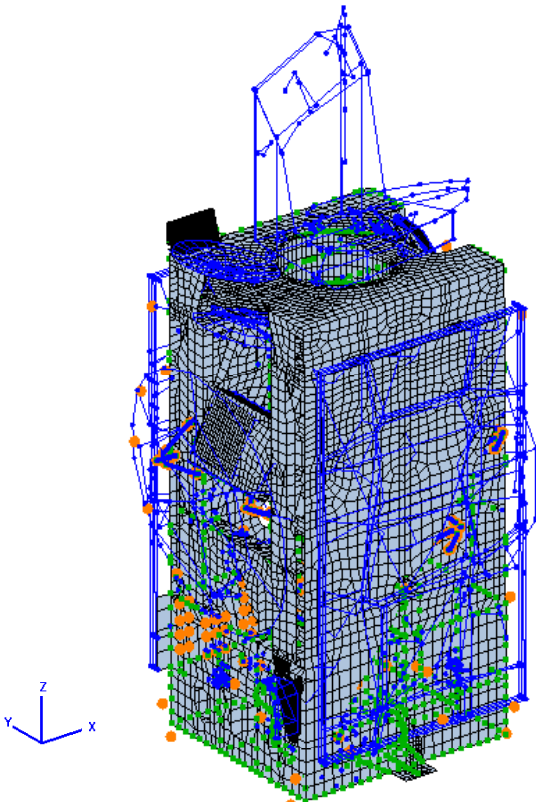
FIG 3.   SPACEBUS 4000 FEM

```
------------------------------
Elements: Mass    :    200
          Spring  :   8691
          Bar     :   5528
          Plate   :  16977
          ----------------
          Total   :  31396
Nodes:    Physical:  22507
          Scalar  :    308
          ----------------
          Total   :  22815
Dofs:     M set   :   4994
          A set   : 108031
          S set   :  22325
          J set   :      6
          ----------------
          Total   : 135350
Modes:    Junction:      6
          Rigid   :      0
          Elastic :    172  (12.4-80 Hz)
          Pseudo  :      0
          ----------------
          Total   :    172
------------------------------
```

TAB 3.   FEM description

3.4. FEM updating

The initial FEM has been compared with the identified modal basis. It was decided to update the FEM stiffness matrix in order to correlate test and analysis results. Some physical zones have been updated according to their corresponding modal energies in the identified modes. It was thus implicitly assumed that these zones were the most likely to influence the global natural frequencies and modes shapes.

The convergence criterion was the error in frequency and the MAC. The results is illustrated hereunder by a MAC matrix (FIG 4) between analysis modes and test modes (called Reference) identified on X axis (see §3.2). Red color stands for high values of MAC (near 1) whereas blue color stands for low values (near 0).
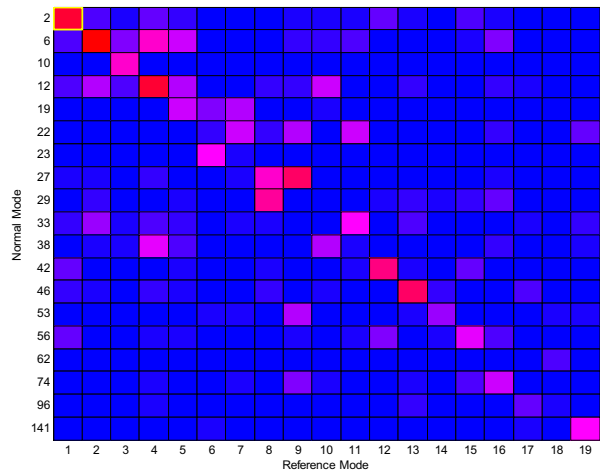
FIG 4.   MAC matrix

```
---------------------------------------------
Model: satA_modal_10_80_ese_correle
Ref. : satA_run_x_LF5_OR025
---------------------------------------------
   Model          Reference       Freq.     MAC
  No.  (Hz)       No.  (Hz)      (% Err)
---------------------------------------------
    2   13.84       1   13.89     -0.36     0.89
    6   22.26       2   22.61     -1.55     0.96
   10   23.11       3   24.02     -3.81     0.58
   12   24.91       4   25.26     -1.37     0.88
   19   28.54       5   27.01      5.67     0.40
   23   29.68       6   28.85      2.86     0.47
   22   29.46       7   29.79     -1.10     0.35
   29   31.89       8   31.51      1.22     0.68
   27   31.58       9   32.55     -3.00     0.62
        .
        .
        .
---------------------------------------------
```

TAB 4.   Comparison between FEM-Test

Some modes are well identified and correlated either in frequency and MAC. The evolution between the initial model and the updated one for the modes identified on X axis is illustrated in FIG 5.

Comparison % Error in frequency - X Axis

Comparison MAC - X Ax is
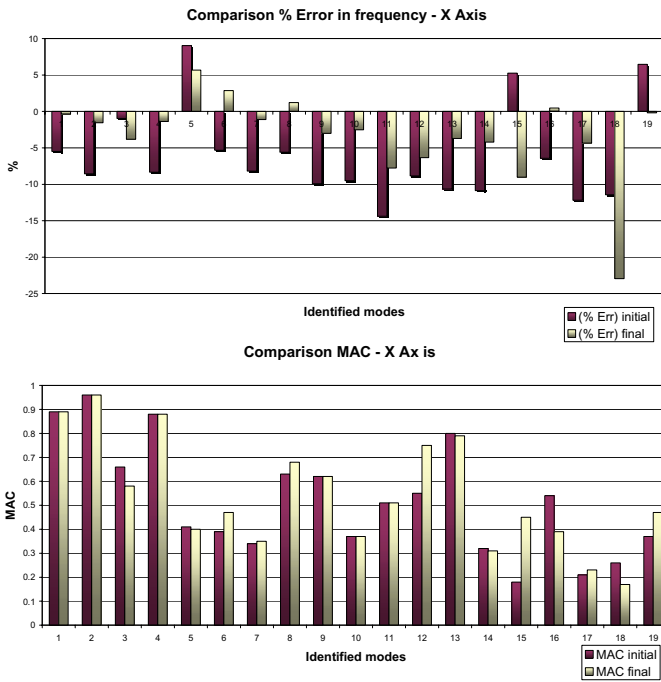
FIG 5.   Comparison before and after FEM updating

The frequency error has been drastically reduced whereas the MAC values were conserved or slightly improved. This result is logical as it is much more difficult to influence a mode shape than a natural frequency. The variations of physical parameters to update the FEM is comprised between –17% to +17%. These variations seem realistic if one considers the :

- • Usual assumptions of average or minimum values (geometry, Young modulus …) in a FEM,

- • Equivalent representation of simplified or non modelled substructures (equipment, neutral axis offsets …) that can locally influence the stiffness matrix.

 The conclusion of this first phase is that the FEM is judge reliable for modal energy estimation.

3.5.   Modal strain energy computation

The retained zones for the identified modes have more than 1% of strain energy. FIG 6 shows an example of the first lateral mode where all the zones with more than 1% of modal strain energy are selected and displayed.
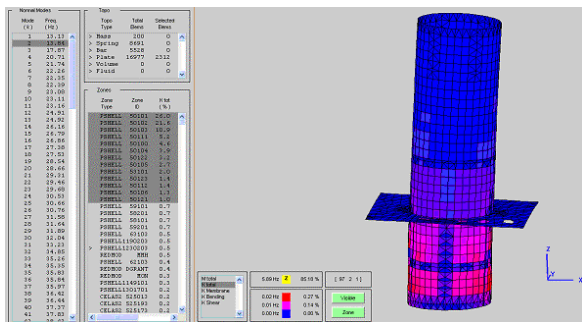
FIG 6.   Zones with more than 1% of energy

The total number of zones is equal to 23 as described

hereunder in TAB 5.

Zones names	Zones description
ABM40	Apogee Boost Motor
CELAS	Links
CT	Central Tube
DGRANT	Earth Antenna
EASTREF	East Reflector
EFMP	Main Plate Feed East
EFSW	Feed Support East
ID	Internal Deck
MMH	MMH Tank
MON	MON Tank
NCMP	North CM Panel
NCMW	North CM Web
NORTHSA	North Solar Array
NSMBP	North Battery Panel
NSMP	North SM Panel
NSMW	North SM Web
SCMP	South CM Panel
SCMW	South CM Web
SOUTHSA	South Solar Array
SSMBP	South Battery Panel
SSMP	South SM Panel
SSMW	South SM Web
WESTREF	West Reflector

TAB 5.   Zones description

It has to be noted that most of the modal strain energy is concentrated on a few number of zones. For instance, for the modes identified on the X axis, 5 zones only have more than 10% of strain energy on at least one mode.

Remark : North and South corresponds to the Y axis (perpendicular to Solar Arrays)

3.6.   Local damping extraction

3.6.1.   Inverse problem characteristics

From the different modes identified along the three axes and the selected zones, one can build the inverse problem with $[\tau_{ks}]$ of size 39 modes x 23 zones. When a given mode has been identified on several axes, it was decided to use a weighted sum between corresponding MAC and frequency error to choose correctly the best one. $[\tau_{ks}]$ is relatively sparse :

- • 163/897=18% of $[\tau_{ks}]$ elements are superior to 1% (as illustrated on FIG 7).

- • The condition number of $[\tau_{ks}]$ is approximately 5000.

- • The last five singular values are inferior to 0.01 with a minimum value of 6e-4.

According to the parameters defined in paragraph 2.5.2, the inverse problem of equation (1) is ill-posed. The least squares solution is not adapted to solve correctly the problem. Regularization is consequently necessary.
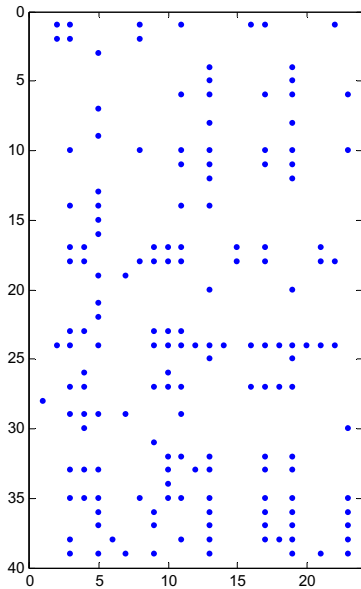
FIG 7.   Matrix $[\tau_{ks}]$

3.6.2. Choice of regularizing operator L

Some supplementary physical equations are added to the initial problem by assuming the equality between some damping coefficients :

$$(5) \quad \begin{cases} \eta_{SOUTHSA} = \eta_{NORTHSA} \\ \eta_{EASTREF} = \eta_{WESTREF} \\ \eta_{MMH} = \eta_{MON} \\ \eta_{NSMP} = \eta_{SSMP} \\ \eta_{SSMBP} = \eta_{NSMBP} \end{cases}$$
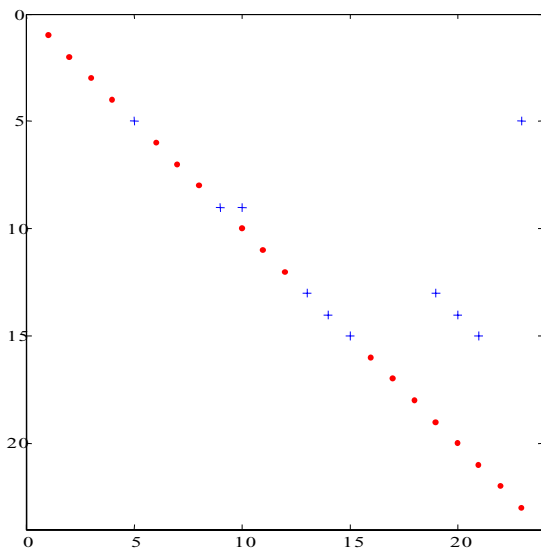
FIG 8.   Regularizing operator L representing equation (5)

Remark : the red elements are equal to 1. The blue ones are equal to 10. The others are null. The value of 10 has

been chosen after numerical iterations to find a compromise between supplementary equations and zones with no added information.

The operator $L = I_n$ has also been tested. It consists in minimizing the 2-norm of the solution, which can be considered as conservative but does not rely on physical considerations. Consequently, this operator was rejected.

3.6.3.   Numerical results

Several cases have been computed.

3.6.3.1.   Case 1 : full matrix $[\tau_{ks}]$

This first case is interesting since it applies the regularization method to the complete problem without any consideration on the identified modes or zones. FIG 9 shows the L-curve defining the parameter λ (see §2.5.2).
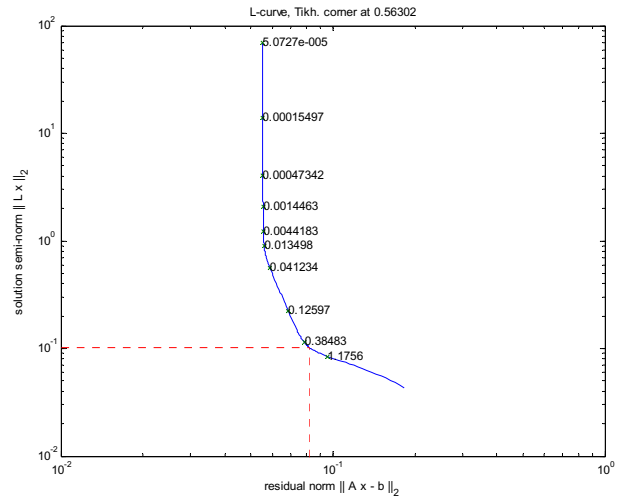
FIG 9.   Case 1 : L-curve for parameter λ

Names	Zones	η
Apogee Boost Motor	ABM	0.013
Central Tube	CT	0.025
Earth Antenna	DGRANT	0.014
East Reflector	EASTREF	0.055
MMH Tank	MMH	0.023
MON Tank	MON	0.023
North CM Panel	NCMP	0.036
North Solar Array	NORTHSA	0.064
North SM Panel	NSMP	0.023
South Solar Array	SOUTHSA	0.063
South CM Panel	SSMP	0.023
West Reflector	WESTREF	0.053

TAB 6.   Case 1 : Local damping results

The damping of the other zones have not been identified because the associated modal strain energy was too low.

3.6.3.2. Case 2 : Modes having MAC > 0.7

This second case considers only modes that are well correlated between test and FEM. The idea is to minimize the sources of error in matrix $\left[\tau_{ks}\right]$. In that case, the matrix is of size 11 modes x 17 zones and is still relatively sparse (21 % of elements with more than 1% of strain energy). FIG 10 shows the L-curve defining the parameter λ (see §2.5.2).
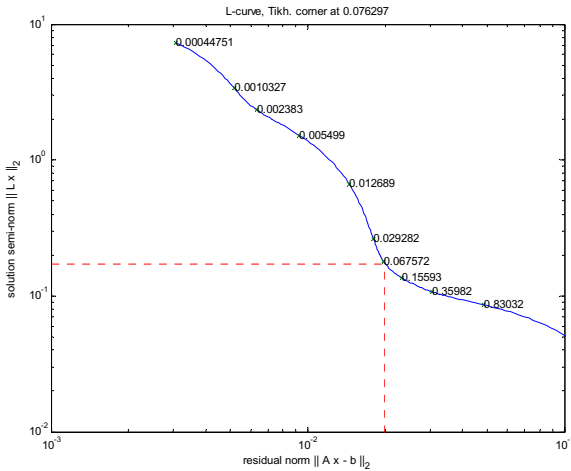
FIG 10.   Case 2 : L-curve for parameter λ

Names	Zones	η
Central Tube	CT	0.03
Earth Antenna	DGRANT	0.057
East Reflector	EASTREF	0.072
MMH Tank	MMH	0.023
MON Tank	MON	0.023
North CM Panel	NCMP	0.036
North Solar Array	NORTHSA	0.076
South Solar Array	SOUTHSA	0.076

TAB 7.   Case 2 : Local damping results

The damping of the other zones have not been identified because the associated modal strain energy was too low.

The MAC sensitivity shows the following :

- Zones for which the damping is relatively stable (e.g. Central Tube)

- Zones for which variations are not negligible (e.g. Earth Antenna)

The possible explanations of such findings are :

- Either modes with MAC < 0.7 are too inaccurate and disturb the matrix $\left[\tau_{ks}\right]$. These uncertainties only concern the model itself. They do not impact the right hand side of equation (1) η_k .

- Either these latter modes are generally located at higher natural frequencies and correspond to

solicitations associated to different damping.

3.6.3.3. Case 3 : Damping function of frequency

The third case explores the latter assumption, i.e. that the damping may depend on the frequency for some zones. In other words, this third case tries to explain the difference between case 1 and 2 by a dissimilar behaviour of some zones between low and high frequencies. Hence, this case is divided into two numerical applications corresponding to modes with natural frequencies below 50 Hz and those with natural frequencies above 50 Hz. FIG 11 shows the dependency of the MAC versus the natural frequencies of the modes. As it can be foreseen, the global shape of this experimental cloud shows a relationship where MAC is inversely proportional to natural frequencies. It just results in the fact that the first modes are better modelled and predicted than the followings.
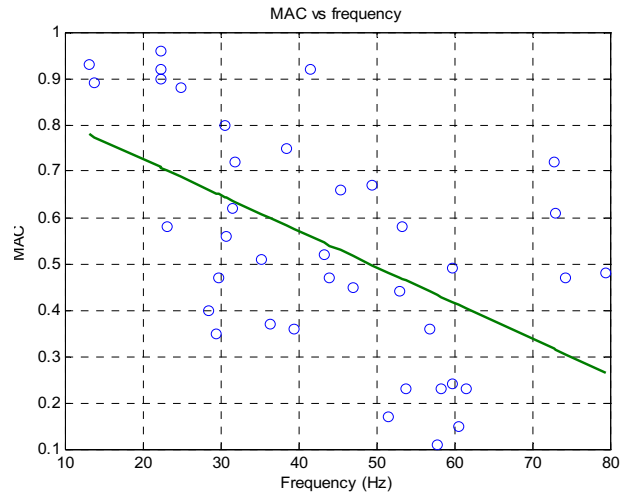
FIG 11.   MAC vs frequency

a)   Modes with natural frequencies below 50 Hz

The matrix $\left[\tau_{ks}\right]$ is of size 24 modes x 21 zones and is still relatively sparse (18 % of elements with more than 1% of strain energy). FIG 12 shows the L-curve defining the parameter λ (see §2.5.2).

Names	Zones	η
Central Tube	CT	0.028
Earth Antenna	DGRANT	0.026
East Reflector	EASTREF	0.06
North CM Panel	NCMP	0.037
North Solar Array	NORTHSA	0.071
North SM Panel	NSMP	0.064
South CM Panel	SCMP	0.03
South Solar Array	SOUTHSA	0.07
South SM Panel	SSMP	0.064
West Reflector	WESTREF	0.059

TAB 8.   Case 3a) : Local damping results
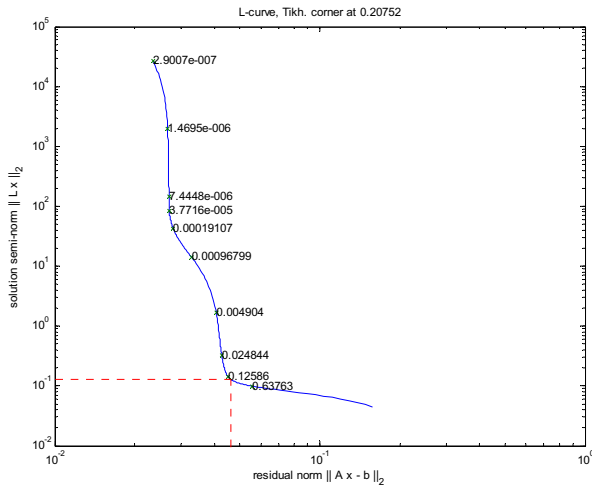
FIG 12.   Case 3a) : L-curve for parameter λ

The damping of the other zones have not been identified because the associated modal strain energy was too low.

The trade-off between residual norm (abscissa of FIG 12) compared to the semi-norm of the regularized solution (ordinate of FIG 12) is clearly visible.

        b)   Modes with natural frequencies above 50 Hz

the matrix $\left[\tau_{ks}\right]$ is of size 15 modes x 13 zones and is still relatively sparse (23 % of elements with more than 1% of strain energy). FIG 13 shows the L-curve defining the parameter λ (see §2.5.2). It can be seen that the L-curve is quite degenerated in that case, meaning that the regularization may not be as efficient as expected. It can confirm the idea that for lower MAC, the sources of error are maybe higher in matrix $\left[\tau_{ks}\right]$, leading to an ill-posed problem that is difficult to regularize.
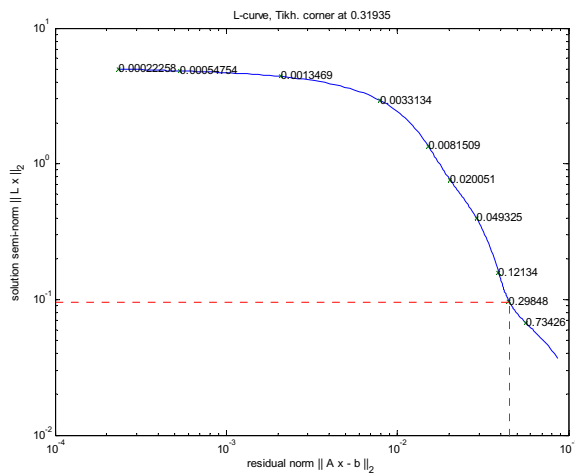
FIG 13.   Case 3b) : L-curve for parameter λ

The damping of the other zones have not been identified because the associated modal strain energy was too low.

Names	Zones	η
Apogee Boost Motor	ABM	0.018
Central Tube	CT	0.012
Earth Antenna	DGRANT	0.02
East Reflector	EASTREF	0.039
MMH Tank	MMH	0.026
MON Tank	MON	0.026
North CM Panel	NCMP	0.056
North Solar Array	NORTHSA	0.049
South Solar Array	SOUTHSA	0.048
West Reflector	WESTREF	0.038

TAB 9.   Case 3b) : Local damping results

3.6.3.4.   Synthesis

Zones	η all modes	η MAC>0.7	η Modes<50 Hz	η Modes>50 Hz
ABM	0.013	-	-	0.018
CT	0.025	0.03	0.028	0.012
DGRANT	0.014	0.057	0.026	0.02
EASTREF	0.055	0.072	0.06	0.039
MMH	0.023	0.023	-	0.026
MON	0.023	0.023	-	0.026
NCMP	0.036	0.036	0.037	0.056
NORTHSA	0.064	0.076	0.071	0.049
SCMP	-	-	0.03	-
NSMP	0.023	-	0.064	-
SOUTHSA	0.063	0.076	0.07	0.048
SSMP	0.023	-	0.064	-
WESTREF	0.053	0.071	0.059	0.038

TAB 10.   Synthesis of extracted damping per zones

The computed values seem physical :

• The central tube is slightly damped in line with its monolithic structure

• Appendices of big area have a relatively high damping (Solar Arrays, Reflectors) that can be linked to the air effect

• Tanks are slightly damped (aluminium structure with a small number of links)

• Synthesized damping decrease generally with frequency, notably for the appendices. The air effect decrease when displacements are small.

• Damping that are not extracted and/or that present high variability from one case to another have to be considered cautiously. It seems that the regularization of the problem is not sufficient to stabilize the solution for these zones.

These values differ sensibly of the usual value of modal

damping, i.e. 2% (η=0.04)

As a conclusion, the damping value to select for a given zone will depend on its use. One can prefer to minimize these values to remain conservative or privilege the values issued from well correlated modes (MAC > 0.7). One can also consider different values depending on frequency.

It is very important to notice that the calculated local damping take into account non modelled characteristics (cabling, equipment, thermal control, links, boundary conditions …) by the mean of η_k. Finally, one does not look for modelling these complex characteristics but to include their effect on damping into the existing FEM.

4. CONCLUSIONS AND FUTURE WORK

The obtained results are encouraging. The numerical applications give realistic order of magnitude, even if a variability according to the assumptions has been put into evidence. An automated method of local damping extraction has been established. This method contains some limitations linked to the uncertainties inherent to the FEM and to the global structural damping extracted during the modal identification process. The supplementary physical information is necessary to the stabilization of the problem and constitutes also an important limitation because these equations are generally in reduced number.

Conversely, one of the undeniable advantages of this method is to associate on one hand the mathematical model that stands for a simplified reality and on the other hand measures on the real specimen giving access to the effect of damping of non modelled parameters (cabling, equipment, thermal control, links, boundary conditions …). These parameters have a non negligible influence on damping and cannot be modelled simply.

Future work will comprise two different aspects. The first one is to include the extracted damping into the correlated model to compare the analytical FRFs to those measured. The second one and probably the most important is to be able to predict these local damping for similar structures by means of influent parameters. Simple rules have to be built thanks to the obtained results.

5. ACKNOWLEGDMENTS

6. ACRONYMS

FEM   Finite Element Model

FRF   Frequency Response Function

MAC   Modal Assurance Criteria

RTMVI Real Time Modal Vibration Identification

SVD   Singular Value Decomposition

7. REFERENCES

[1] Girard A., Roy N. , Dynamique des structures industrielles, Lavoisier, 2003

[2] Hansen Per Christian, Regularization Toolbox, A Matlab Package for Analysis and Solution of Discrete Ill-Posed Problems, Version 3.1, Sept 2001

[3] Bonnet M., Problèmes inverses, DEA Dynamique des Structures et Couplages, Oct 2004

[4] Roy, N., PRIMODAL® User's Manual V1.4, 2006

[5] Girard A., Roy N., Guyot M., Bugeat L.P., Modal identification via effective parameters : an industrial solution, European Conference on Spacecraft Structures, Materials and Mechanical Testing, Dec 2000, ESA

[6] Nelder, J. A., Mead, R., A Simplex Method for Function Minimization, Computer Journal, Vol. 7, Issue 4, January 1965, pp. 308-313.